Environmental Pollution 330 (2023) 121751

Contents lists available at ScienceDirect

Environmental Pollution

journal homepage: www.elsevier.com/locate/envpol

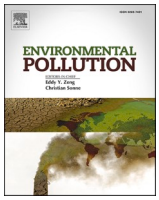

Facile one-step synthesis of a versatile nitrogen-doped hydrochar from olive oil production waste, "alperujo", for removing pharmaceuticals from wastewater

S. Escudero-Curiel *, M. Pazos, A. Sanromán

CINTECX. Universidade de Vigo, Department of Chemical Engineering. Campus As Lagoas-Marcosende, 36310, Vigo, Spain

ARTICLE INFO

Keywords:
Nitrogen-grafting
Polyethyleneimine
Urea
Adsorption
Pharmaceuticals
Water treatment

ABSTRACT

In line with the principles of zero waste and recycling, alperujo (AL) was used in this study to produce a value-added product: hydrochar (HC) with high adsorption capacity. An optimization of the hydrothermal carbonization (HTC) conditions, such as temperature, residence time, and water/solid ratio, was carried out to maximize the adsorption capacity. Eight HCs were obtained, and an in-depth comparative characterization, as well as adsorption tests of two pharmaceuticals with very different physicochemical properties (fluoxetine (FLX) and cefazolin (CFZ)), were performed. This first step allowed for elucidation of the best candidates to carry out nitrogen grafting on their surface, resulting in the HC obtained at a higher water/solid ratio and temperature, and longer residence time: 3-220°C-2.5 h with a maximum uptake of 4.6 and 0.4 mg/g for FLX and CFZ, respectively. After that, a facile one-step, one-pot synthesis of nitrogen-doped hydrochars (N-HC) was developed to prepare a versatile bio-adsorbent with enhanced adsorption capacity. Two N–HCs were prepared using urea (U-HC) and polyethyleneimine (PEI-HC) and were intensively characterized to shed light on the adsorption mechanism. In both cases, amide groups were formed, which favored the adsorption process. PEI-HC acquired an outstanding maximum adsorption capacity of 983.84 mg/g for CFZ, and 29.31 mg/g for FLX, and the process was well described by the Freundlich isotherm and pseudo-second-order kinetic model. A co-adsorption test was performed using PEI-HC for both pharmaceuticals, finding that the adsorption process occurs in different active sites because there was no interference between the pollutants. This fact corroborates the versatility of the new bio-adsorbent synthesized.

1. Introducction

The effects of pharmaceuticals in flora and fauna are varied and complex, ranging from acute or chronic when these compounds are released into the environment mainly from excretion, as the drugs are not completely metabolized (Ebele et al., 2017). Nowadays, a lack of official regulations that control its release to the environment makes it difficult to monitor pharmaceuticals and assess their impact on aquatic ecosystems and human health (Ewadh et al., 2017). Nevertheless, concerns about the release of these compounds into the environment have increased worldwide (Melchor-Martínez et al., 2021), and it is only a matter of time before the competent authorities act and begin to regulate (Ewadh et al., 2017).

To date, the scientific community has tested many techniques with varying degrees of success in order to be prepared for when their implementation in wastewater treatment plants (WWTPs) will become necessary. In this respect, adsorption processes have shown particularly reliable results, proving to be remarkably effective even on an industrial scale (Ahmed and Hameed, 2018). If this technique stands out among many others, it is because of its simplicity of operation, high performance, and its great cost-effectiveness (Rajapaksha et al., 2019). As a result, the search for adsorbent materials is constantly growing. Adsorbents from agro-industrial origin, or bio-adsorbents, are one of the best bets, in the interest of generating value-added products considering the principles of zero waste and recycling (Mohan et al., 2014). Most of these bio-adsorbents possess a high content of cellulose, hemicellulose, and lignin, which makes them perfect precursors for HC production (Reza et al., 2014). HC adsorption capacity is strongly influenced by the raw material and the HTC conditions applied, mainly temperature, residence time and water/solid ratio (Delgado-Moreno et al., 2021). In

* Corresponding author.
E-mail address: sescudero@uvigo.gal (S. Escudero-Curiel).

https://doi.org/10.1016/j.envpol.2023.121751
Received 4 January 2023; Received in revised form 1 April 2023; Accepted 28 April 2023
Available online 5 May 2023
0269-7491/© 2023 The Authors. Published by Elsevier Ltd. This is an open access article under the CC BY-NC-ND license (http://creativecommons.org/licenses/by-nc-nd/4.0/).

addition, the great content in reactive groups on the outer surface of the HC (Jiang et al., 2019), makes it a customizable surface on which different functionalization can be performed to improve its adsorption efficiency (Rajapaksha et al., 2016). This is particularly attractive from the viewpoint of industrial applications, since pharmaceuticals are a diverse group of organic compounds that can be found in many forms and ionized species in wastewater. Thus, engineered HC may solve affinity problems between bio-adsorbents and target pollutants as has been described in recent studies included those by Ahmed et al. (2023), Barjasteh-Askari et al. (2021), Choudhary and Philip (2022) and Xie et al. (2023). Despite variations in the types of adsorbents used and the methods of functionalization employed, the aforementioned studies reported improvements in adsorption capacity of their respective target substances.

Surface grafting is one of the cutting-edge techniques applied in the development of engineered adsorbents (Deng and Ting, 2005; Rajapaksha et al., 2016). Tailoring materials is often done with anionic or cationic surfactants and nitrogen-rich compounds such as urea (U), ammonia or polyethyleneimine (PEI) (Elsayed et al., 2022). Surface grafting with nitrogen-rich compounds brings nitrogen-containing functional groups onto the carbon surface, such as NH_2, amides, pyridinic, pyrrolic and graphitic nitrogen groups (Arrigo et al., 2010). In addition, the electronic properties of a nitrogen-doped (N-doped) surface, localized charge accumulation, contribute to electron transfer reactions and assist in the adsorption and/or dissociation of molecules (Yang et al., 2014). Nitrogen-doping or nitrogen-grafting has attracted increasing attention due to its efficient surface modification, and some carbonaceous materials have been modified with nitrogen-rich compounds for adsorption purposes (Deng and Ting, 2005; Jiang et al., 2019; Kasera et al., 2021; Xiao et al., 2020), however, the techniques applied for surface grafting are usually time-consuming treatments involving the use of solvents or other strong oxidizing chemicals (Chen et al., 2020; Huang et al., 2018; Qu et al., 2023; Xia et al., 2020). Therefore, finding a new method of synthesis that is more facile and versatile is important, as it would enable a simpler and more efficient production process while reducing environmental impact and maintaining the quality of the final product.

AL, obtained from olive oil two-phase extraction process, is the principal waste produced by this important industry. AL is a lignocellulosic waste with a high organic matter content. Its water content is typically ranging from 50 to 80% and is rich in phenols (Alburquerque et al., 2004) that cannot be discharged freely due to its toxic properties, acidity and its extremely high biological and chemical oxygen demand (Aharonov-Nadborny et al., 2016). On the other hand, some uses have been attempted for this waste, such as agricultural recycling and co-composting, but they have proved impractical and expensive (Rinaldi et al., 2003). Consequently, AL could be a suitable candidate for HC production and subsequent N-doping. Thus, AL is considered a waste product and has low economic value, which makes it an attractive feedstock for producing HC, as it can be obtained at a relatively low cost. On balance, using AL as a feedstock for HC production can help reduce waste and create value from an otherwise low-value by-product. In addition, the Food and Agricultural Organization of the United Nations acknowledges the importance of addressing the environmental impact of food waste through measures such as prevention, reduction, reuse, and recycling. These actions are seen as essential steps towards achieving greater sustainability in the food industry and reducing the ecological footprint of food production and consumption (Opatokun et al., 2015).

To our knowledge, there are scarce research articles trying to valorize AL as HC or biochar with adsorption purposes in the last 5 years (Delgado-Moreno et al., 2021; Gimenez et al., 2020; González and Manyà, 2020). This study aimed to optimize the HTC conditions to produce HCs that can effectively remove two pharmaceuticals with different physicochemical properties, namely FLX and CFZ. The use of these widely prescribed pharmaceuticals allows for testing the versatility and effectiveness of the HC in treating a range of contaminated water sources. This approach also enables identifying any potential limitations or challenges associated with the HC's use, which is crucial for informing future research and development efforts. To overcome the limitations and enhance adsorption properties for pharmaceuticals, two different nitrogen sources, U and PEI, were incorporated into the production of the HC with the best adsorption performance to synthesize a versatile engineered bio-adsorbent from AL in a facile one-pot, one-step process. The use of environmentally friendly nitrogen sources also highlights the potential for sustainable and cost-effective production of engineered adsorbents. Overall, the findings of this study can inform the development of more efficient and sustainable approaches for treating contaminated water sources and managing industrial waste, so that two environmental problems, industrial waste management and removal of emerging pollutants, could be addressed at the same time. The versatility and effectiveness of the N-HC in treating contaminated water sources, along with its potential to address two environmental problems simultaneously, underscore the relevance of this study.

2. Materials and methods

2.1. Reagents and solutions

AL was kindly provided by Aceites Abril S.L. (Ourense, Spain). FLX as Fluoxetine hydrochloride (Sigma-Aldrich) and CFZ (Supelco) were purchased in the grade of secondary pharmaceutical standard. U and PEI (branched, M.W 10,000, 99%) were obtained from VWR International and Alfa Aesar respectively. Stock solutions of FLX, CFZ and FLX-CFZ were prepared in distilled water and kept refrigerated at 6 °C until further use.

2.2. HTC process

HCs were produced in a cylindrical hydrothermal reactor made of stainless steel with a 100 mL PTFE inner chamber under autogenic pressure. Briefly, to simulate a Water (W)/AL ratio of 3 or 2, dried AL were placed inside the PTFE chamber and covered with distilled water to reach a total amount of 50 g inside the chamber in both cases. Partially based on the findings of Atallah et al. (2019) and Missaoui et al. (2017), with some modifications, combinations of two temperatures (160 °C, 220 °C), two residence times (1.5 h, 2.5 h) and two W/AL ratios (3 and 2) were used to obtain a sample set of 8 HCs. The obtained HCs were named as follows: A-B-C where A represents the W/AL ratio, B represents the temperature, and C represents the residence time. The values were selected After the HTC process, all HCs were dried overnight in an oven at 50 °C, sieved and stored for further use.

2.3. One-step, one-pot nitrogen-grafting process

N-HC were prepared similarly as prior described in section 2.2. To establish the mass ratio in our methodology, two previous studies were taken into account (Chen et al., 2020; Rosli et al., 2019), with some modifications to suit the objectives of our research. Shortly, 25 g of PEI and U were first dissolved in 37.5 g of distilled water and subsequently, 12.5 g of AL was added to the mixture in such a way as to obtain an AL/U or AL/PEI mass ratio of 1:2 inside the PTFE inner chamber. The resulting N–HCs were named by adding PEI or U before A-B-C to identify the HTC conditions and the nitrogen source. After the HTC process, the N–HCs were washed three times with plenty of distilled water to remove any unreacted nitrogen source (using warm water in the case of PEI), filtered, and then dried overnight in an oven set at 50 °C. Next, the N–HCs were sieved and stored in zip-lock bags for further use.

2.4. Characterization

This section is described in detail in the Electronic Supplementary Material (ESM).

2.5. Evaluation of adsorption capacity and kinetic studies

All materials, AL precursor and the synthesized HCs were tested separately for FLX and CFZ adsorption. In short, 25 mL of FLX or CFZ (30 mg/L) were placed in a cylindrical, amber-colored tube and subsequently, 0.125 g of each adsorbent was introduced inside the tube. The mixture was put into agitation in a rotary shaker at 100 rpm for 24 h (Roller shaker 10 basic IKA®). For evaluating the maximum adsorption capacity, different amounts of the selected HC were placed inside the amber-colored tubes whereas the concentration of the pollutant was maintained. Langmuir and Freundlich isotherms models were selected to fit the experimental data. To study the reaction kinetics, samples were taken at regular intervals of time for 24 h. Both pseudo-first (PFO) and pseudo-second-order (PSO) kinetic models were chosen for fitting the collected data. The isotherm and kinetic model equations for fitting the data are presented in Table 1. All samples were filtered through PTFE hydrophilic syringe filters (0.45 μm pore size) and pharmaceutical concentrations were analyzed by high performance liquid chromatography equipment (HPLC) equipped with a diode array detector (Infinity 1100, Agilent Technologies). HPLC method (validation parameters are presented in Table ESM1) for FLX and CFZ quantification consisted of using a Kinetex® 5 μm Biphenyl 100 Å reversed-phase column and a percentage of Water/Methanol/Ammonium formate of 65/30/5 as mobile phases (analysis for FLX at 228 nm and for CFZ at 271 nm).

3. Results

3.1. Characterization of HCs

Table ESM2 shows the elemental composition of the 8 HCs obtained with the different HTC conditions applied. HCs hydrogen content was almost constant in all the samples around 6%, but marginally lower values were observed in samples with a longer residence time for both temperatures tested. The carbon content of the produced HCs increased slightly with the increase in temperature during the HTC process, reaching a maximum of 59.29% for 3-220-2.5 similarly to the results reported by Saha et al. (2019) on cellulose and woods HCs at 180 and 220 °C. It is noteworthy that at the lowest temperature, the change in carbon content was negligible, regardless of the duration of the process. Even though the residence time was 3 and 5 times longer in the present study, these data are in good agreement with those reported by Volpe and Fiori (2017) who argued that almost no changes were observed regarding the raw AL when temperatures of HTC below 180 °C were applied because it was not sufficiently intense to influence substantially the raw materials. Also, the possibly minimal variations could be attributed to the loss of the soluble organic and inorganic fraction that may be present in the AL, which might be between 10 and 12% of the total matter content (Alburquerque et al., 2004). In an HTC process, the first reaction occurring is hydrolysis and this reaction triggers and favors the rest of the reactions that take place in the process such as dehydration, decarboxylation, aromatization and recondensation (Libra et al., 2014). Thus, the water involved in the HTC process not only acts as a solvent and reagent but also as a catalyst for the carbonization process (Reza et al., 2014). However, the steepest rise was observed in the samples that were produced at the highest temperature, highest W/AL and longest retention time. This pattern was also reported by Missaoui et al. (2017) in their study conducted with AL to obtain energy. This fact indicated that temperature was probably the key parameter performing changes in the HCs elemental composition and, once the higher temperature was applied, time proved to be also important for AL modification allowing the hydrolysis reaction and all the other reactions it triggers to take effect on. Regarding nitrogen content, a decrease was observed in the HCs produced with the highest water content. This fact could be ascribed to higher solubilization and hydrolysis of proteins in HCs with a higher W/AL ratio (Capobianco et al., 2020).

Table 1
Equations and parameters of isotherm models and adsorption kinetics.[a]

	Parameters	U-3-220-2.5		PEI-3-220-2.5		PEI-3-220-2.5 (MIX)		FLX
		FLX	CFX	FLX	CFZ	FLX	CFZ	3-220-2.5
Isotherm Models								
Langmuir								
	q_m (mg/g)	111.63	16.09	33.24	1572.73	–	–	44.36
$q_e = \frac{q_{max} * K_L * C_e}{1 + K_L * C_e}$	K_L (L/mg)	0.003	0.06	0.02	0.02	–	–	0.02
	SEE	13.58	0.04	1.39	90.65	–	–	1.43
	R^2	0.983	0.998	0.984	0.822	–	–	0.986
Freundlich								
	K_F (L/mg)	1.23	2.20	3.58	78.95	–	–	0.70
$q_e = K_F * C_e^{\frac{1}{n}}$	n	1.52	2.40	2.57	1.71	–	–	1.60
	SEE	5.34	0.93	1.12	69.55	–	–	2.37
	R^2	0.963	0.974	0.989	0.895	–	–	0.961
Kinetic Models								
PFO								
$q_t = q_e(1 - \exp^{-k_1 t})$	q_e (mg/g)	62.44	12.43	28,13	263.3	28.23	259.36	–
	k_1 (1/min)	0.16	1.27	1.33	0.02	1.21	0.03	–
	SEE	3.61	0.89	1.9	20.62	3.59	25.41	–
	R^2	0.981	0.971	0.957	0.95	0.96	0.72	–
PSO								
	q_e (mg/g)	70.2	13.01	28.8	284.62	28.86	263.86	–
$q_t = \frac{q_e^2 * k_2 * t}{(1 + k_2 * q_e * t)}$	k_2 (g/(mg min))	0.003	0.15	0.07	1.33	0.07	2.68	–
	SEE	2.2	0.53	1.27	9.15	1.37	18.40	–
	R^2	0.993	0.9872	0.981	0.99	0.986	0.797	–

[a] q_e (mg/g) is the adsorption capacity at equilibrium, q_m (mg/g) is the maximum adsorption capacity, K_L (L/mg) is the Langmuir equilibrium constant, C_e (mg/L) is the equilibrium concentration of pollutants, K_F and n are Freundlich constant related to adsorption capacity and the strength of adsorption respectively. q_t (mg/g) is the amount of pollutant adsorbed by HC at time t (min) and k_1 (1/min) and k_2 (g/(mg min)) are pseudo-first and pseudo-second order kinetic constant, respectively.

All produced HCs presented a slightly acid character, with values of point of zero charge (PZC) around 5 and very similar to AL (Table ESM2). These results are often found in HCs regardless of the raw material source (Delgado-Moreno et al., 2021). It may be explained because during an HTC process, the aqueous phase is acidic due to the reactions taking place and the by-products produced during the HCT process, such as carboxylic acids (Reza et al., 2014). These conditions lead to an increase in the capacity of the liquid phase to dissolve and maintain solubilized much of the inorganic fraction of the biomass (acid solvation mechanism) which is the main contributor to the alkalinity of the biomass (Benavente et al., 2015; Delgado-Moreno et al., 2021). In agreement with these findings, Román et al. (2020) indicated that an HC prepared from olive stone at 250 °C similarly presented a PZC of 4.05.

FTIR analyses were performed to identify the changes the AL underwent in the HTC process and the functional groups that could be involved in the adsorption studies and the data are shown in Fig. 1a. AL is essentially composed of lignin (45.8%), hemicellulose (37.7%), cellulose (20.8%), proteins (7.7%), and fats (13%) (Alburquerque et al., 2004). It is therefore not unexpected to observe functional groups connected to these principal constituents. The distinctive peaks linked with the existence of these principal components are outlined in Table ESM3.

The region from 1160 cm^{-1} to 895 cm^{-1} gathers peaks and bands generally dominated by the polysaccharides such as C–O–C ether from the monomer rings at 1160 cm^{-1}, C–O from hydroxyl groups at different carbon positions from 1105 cm^{-1} to 1024 cm^{-1}, and 895 cm^{-1} from the β-O-glycosidic bonds (Xu et al., 2013). The sharpest decrease in these peaks and bands in HCs 3-220-2.5 and 2-220-2.5 indicates the degradation of these components, mainly hemicellulose as is less stable, through decarboxylation and dehydration (Reza et al., 2014). The degradation of the polysaccharides is relevant since the intermediates of thermal degradation of the sugars (furfurals like 5-HMF, erythrose, and aldehydes) undergo subsequent reactions of condensation, polymerization and aromatization that lead to the formation of the HC (Reza et al., 2014).

An increase in C–H bending vibrations usually contributed by cellulose, hemicellulose and lignin was found at 1374.8 cm^{-1} and contributed only by lignin at 1451 cm^{-1} (Xu et al., 2013), meaning a prevalence of lignin over the other two polymers during the HTC process.

The peak at 1738.9 cm^{-1} can be ascribed to the C═O stretching in hemicellulose and ester from aliphatic chains of triglycerides present in AL (Volpe et al., 2018; Volpe and Fiori, 2017). Additionally, the peak around 1695.3 cm^{-1} is attributed to the conjugated C═O stretch of aldehydes, ketones, ester, lactones and carboxyl acids in chars produced from AL during the HTC process and also could be contributed by unconjugated C═O in lignin (Abdelhadi et al., 2017; Delgado-Moreno et al., 2021; Reza et al., 2014).

The peaks at 2852.9 and 2922.7 cm^{-1} are attributed to the C–H stretching vibrations of methylene and terminal methyl groups of fatty acids chains and also a peak at 3012 cm^{-1} (C–H stretching from unsaturated C═C–H) (Abdelhadi et al., 2017). These peaks together with the ester peak at 1738.9 cm^{-1}, therefore, could indicate that the aliphatic structures, mainly residual triglycerides from olive oil, are being conserved during the HTC process in HCs 3-220-2.5 and 2-220-2.5.

Additionally, the peaks at 1271 and 1314 cm^{-1} are mainly contributed by the guaiacyl and syringyl rings from lignin respectively (Xu et al., 2013). Other peaks are as well ascribed to lignin, for instance, the peak at 1595 cm^{-1} is normally related to its aromatic skeletal and phenol-(C═O)- groups and the peak at 1514.6 cm^{-1} with the aromatic skeletal vibration (Xu et al., 2013). Thus, the steepest increment in these peaks together with the greater prominence of a shoulder at 2955.4 cm^{-1} (aromatic sp^2 C–H) might be taken as clues that indicate the increase in the degree of aromatization of 3-220-2.5 and 2-220-2.5.

The broad band around 3299.8 cm^{-1} is related to the stretching vibrations of O–H, which are mainly contributed by hydroxyl or carboxyl groups present in cellulose or lignin phenols and chemisorbed water (Volpe et al., 2018). A reduction is observed for the HCs produced at the highest temperature and the longest residence time, which may be ascribed to AL dehydration reactions that took place during the HTC process. These results are in agreement with similar results reported by several studies when preparing HC from AL (Gimenez et al., 2020; Volpe et al., 2018) and also are in accordance with those indicated by the elemental analysis. Therefore, it was confirmed the highest degree of carbonization of the HCs produced at the highest temperature and longest time, 3-220-2.5 and 2-220-2.5, the same as the results reported by Missaoui et al. (2017). In addition, a large number of functional groups, particularly those containing oxygen and hydrogen, would enable the interaction between ionic and polar compounds in the event of adsorption and/or a grafting process (Liu et al., 2010).

Considering the whole range of the spectra (400-4000 cm^{-1}), a PCA was applied to the FTIR spectra obtained for all HCs (Fig. 2). This statistical technique is applied to visually extract and interpret the most significant variations in the FTIR spectra, the principal components (PC), and to identify the factors causing this differentiation (Popescu et al., 2013). In this study, 87.5% of the total variability in the spectra is explained by two PC: PC1 65.5% and PC2 22%. The loading plots for PC1 and PC2 are useful to perceive which wavenumbers contribute most to the total variability in the spectra and in what magnitude and direction (increase/decrease). These loading plots can be found in Fig. ESM1a and ESM1b respectively.

Given that PC1 captures the majority of the significant changes in the spectra, it is important to acknowledge that AL is situated at the leftmost point of the plot, and that all HC scores are shifting towards the right of it on the PC1 axis to varying degrees. HCs produced at 160 °C are slightly rightward shifted on the axis PC1 with respect to AL for both treatment residence times 1.5 and 2.5. However, the HCs produced at 220 °C are strongly shifted to the right, remarkably more for treatment times of 2.5 h than 1.5 h. Regarding the W/AL ratio, the lowest coefficients lead to slight rightward shifts in PC1 for all samples. The loading plot for PC1 showed that a rightward shift in PC1 can be associated with substantial degradation of polysaccharides, which dominated the region 1162-826 cm^{-1} together with the broad peak of –OH on 3000-3500 cm^{-1} had the most negative values. Later, this removal of polysaccharides leads to an increase of lignin (broad peak 1700-1680 cm^{-1} C═O groups, 1595 cm^{-1} and 1515 cm^{-1} mainly) and lipid content (3000 cm^{-1}, 2850- 2750 cm^{-1}) towards the right direction in PC1 axis, being the HCs produced at 220 °C and 2.5 h the furthest away from AL.

When it comes to PC2, it is observed that shifts towards the upper part of the PCA plot, where AL is located, are attributed to a higher contribution of discrete peaks of different magnitudes in the region 1100-870 cm^{-1}. Since that region is mainly dominated by polysaccharides, it can be interpreted that the HCs at 160 °C underwent differential degradation of the different polysaccharides. Note that hemicellulose, lignin and cellulose in HTC treatments start to decompose at 180 °C, 180-220 °C and above 220 °C respectively (Reza et al., 2014). As evidence of this, the band found at 1235.5 cm^{-1}, which is specific to C–O–C of xylose is gathered by PC2 with positive values. Therefore, HCs at 160 °C located in the most negative part of PC2 have less contribution of this peak because there is probably degradation of hemicellulose. In addition, the bands of amide I, 1652 cm^{-1}, and amide II, 1542 cm^{-1}, and C–N 1400 cm^{-1} related to proteins are reduced in a downward direction from PCA plot, implying protein removal.

In general, there is a good correlation between the temperature and residence time used for the HTC treatments and the two main peaks related to aromaticity, 1595 cm^{-1} and 1515 cm^{-1}. Figure ESM2 shows how the aromaticity increases from AL to the rest of the HC synthesized. Aromaticity increases greatly when a higher temperature is applied followed by increases in the time of the treatment. This increase in aromaticity can be associated with the permanence of lignin and the char formation after the treatment.

Giving the characterization tests performed on the HCs, in which the

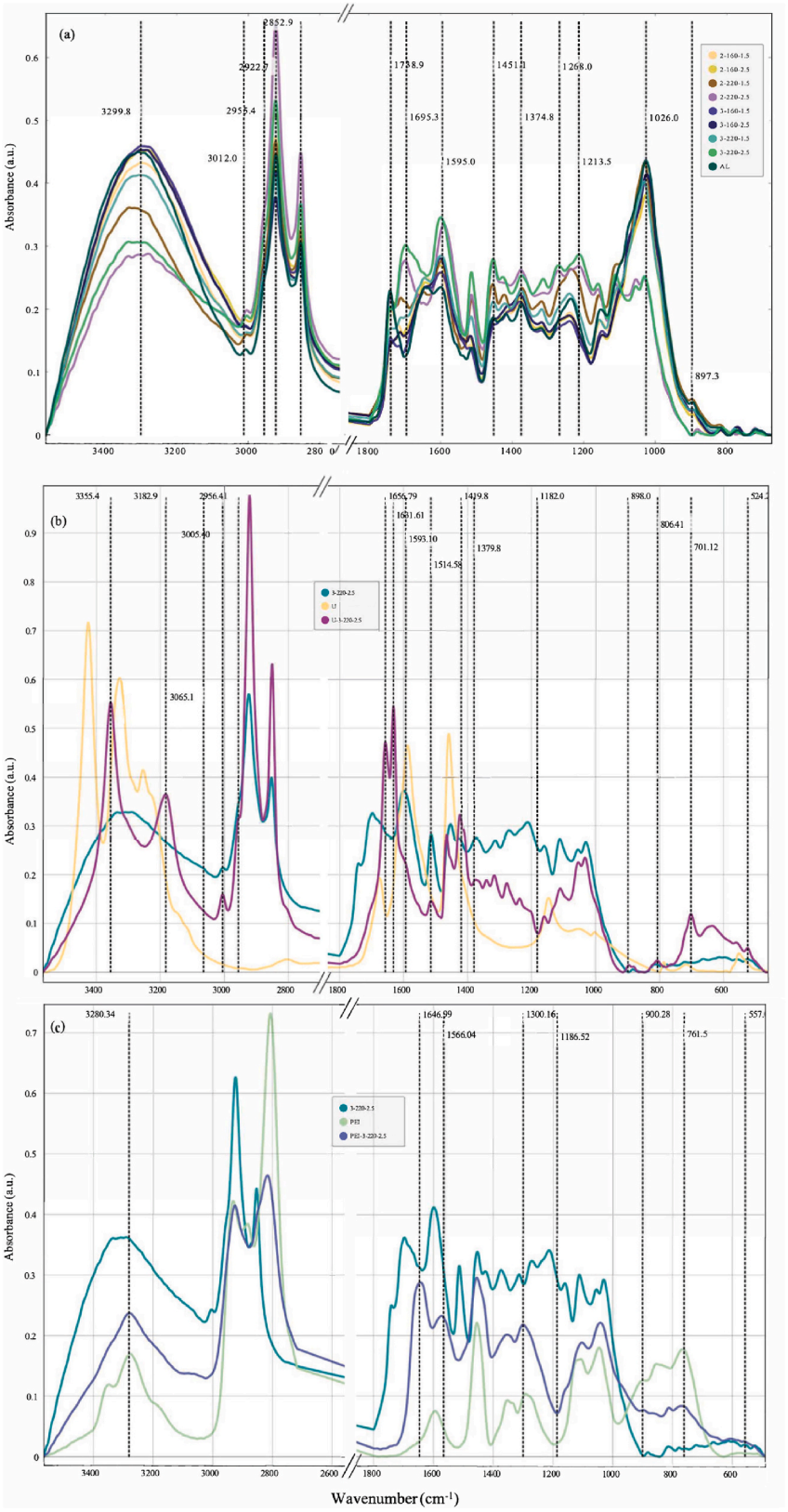

Fig. 1. FTIR spectra of all HCs produced at the different temperatures, residence time and W/AL ratio (a), N-HC with the nitrogen source (b) U-3-220-2.5 and (c) PEI-3-220-2.5.

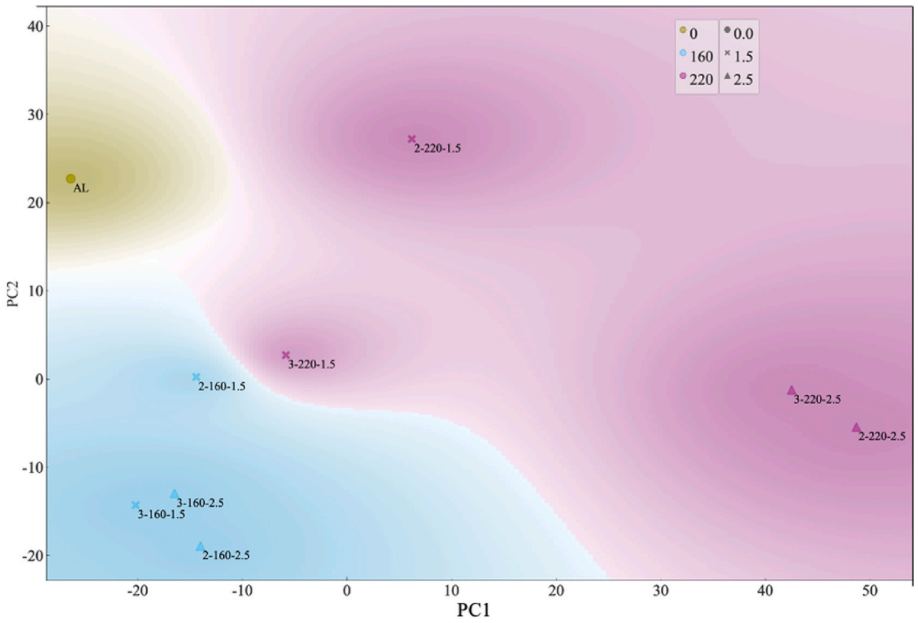

Fig. 2. Score plot of the analysis of PCA representing PC1 vs. PC2 for al HCs produced at the different temperatures, residence time and W/AL ratio.

HCs produced at 220 °C and 2.5 h showed the clearest differences with respect to the original residue, AL, and according to the PCA study almost no differences were found between the samples with W/AL 3 and 2, HC 3-220-2.5 was selected to verify its structure and surface morphology by SEM together with AL. SEM images from raw material, AL, and 3-220-2.5 are presented in Fig. 3a and 3bcd, respectively. AL exhibited a heterogeneous surface with no signs of porosity and after HTC treatment, the changes in its surface structure are more than evident, however, no incipient porosity seems to be discernible. Fig. 3b suggests the appearance of the carbon spheres characteristic of HCs. These carbon spheres are established to possess a core-shell type structure, composed of a hydrophobic core and a hydrophilic shell, in which numerous functional groups such as carbonyl, carboxylic and hydroxyl are present (Jiang et al., 2019). The formation of these spheres, microspheres or nanospheres, is ascribed to polymerization reactions of monomers derived from the hydrolysis of cellulose and hemicellulose present in the precursor material (Reza et al., 2014). Nanospheres are usually interconnected (Gimenez et al., 2020), as in the case of HC 3-220-2.5 (Fig. 3bcd). Delgado-Moreno et al. (2021) reported larger spheres in a HC produced at 240 °C after 6 h of treatment using AL as starting material. Wang et al. (2018) concluded that time was the key parameter governing both the means of dispersion or aggregation and the diameter of these spheres.

BET results are consistent with the SEM images, indicating heterogeneous values for all HCs ranging from 0.45 to 0.02 m^2/g with a standard deviation of 0.18, confirming that HCs did not develop porosity during any HTC treatment. These results are quite lower than those reported by Delgado-Moreno et al. (2021) for a HC of AL produced at 240 °C and 6 h of treatment who achieved a value of 7.62 m^2/g, being probably the time the key parameter since the temperature was similar. In general, HCs do not develop a high specific surface area, unlike chars obtained by pyrolysis (Mumme et al., 2011).

3.2. Adsorption studies

The results of FLX (Fig. 4a) and CFZ (Fig. 4b) adsorption after 24 h showed a good adsorption performance of all HCs with respect to FLX, however, for CFZ the adsorption resulted to be very low. Considering the slightly acidic character of all the HCs, with a PCZ around 5 (Table ESM2), together with the initial pH of the solutions, 6.4 for FLX and 5.9 for CFZ, it was postulated that the net surface charge of the HCs was negative. In this way, at that initial pH FLX with a pKa of 9.4, the –NH group of FLX tends to be protonated, giving a net positive charge to the molecule, thus, electrostatic attraction is favored between this group and the oxygen-reactive species on the HC surface. However, at this pH, the carboxyl group of CFZ with a pKa of 2.84 suffers a deprotonation, which confers a net negative charge to the molecule (see microspecies distribution and molecules of FLX and CFZ in Fig. ESM3), which inhibits the adsorption of CFZ molecules due to electrostatic repulsion. Thus, these results might be explained because of electrostatic interactions between the pollutants molecules and the HCs surface for both FLX and CFZ. HCs 3-220-2.5 and 2–220.2.5 offered the best performance for FLX, with adsorption values of 4.63 and 5.95 mg/g respectively. These results are in good agreement with the FTIR data, where the richness of these samples in functional oxygen-containing groups was indicated. Delgado-Moreno et al. (2021) reported higher maximum adsorption capacity values of 11, 10 and 13 mg/g for diclofenac, ibuprofen and triclosan respectively, which could be related to the develop of more specific surface area, 7.64 m^2/g, of their HCs of AL produced at 240 °C for 6 h and also with a higher PZC. In addition, Román et al. (2020) reported an olive stone HC prepared at 250 °C for 30 min and activated by air for FLX adsorption, achieving a maximum uptake of 44.07 mg/g with a specific surface area of 204 m^2/g.

At this stage, despite 2–220.2.5 appearing to be the most favorable HC, the differences identified by FTIR between HC 3-220-2.5 and 2-220-2.5 were insignificant. Moreover, given that our natural residue, AL, had a high water content of 72%, it was decided to proceed with HC 3-220-2.5 for the subsequent grafting with nitrogen compounds PEI and U. This was done to assess the possibility of enhancing the adsorption capacity of both pollutants.

3.3. N–HCs characterization

Elemental composition of synthetized N-HC, U-3-220-2.5 and PEI-3-220-2.5, is shown in Table ESM2. Although it can be observed a remarkable increase in the nitrogen content in both N–HCs, it is perceived a drastic increase in the nitrogen content in PEI-3-220-2.5. This fact means that the grafting process was very successful in introducing nitrogen in the HCs. The differences could be ascribed to a higher content of nitrogen in the branched polymer. Regarding U-3-220-2.5, similar results were found by Xiao et al. (2020) who prepared a one-pot U-assisted HC from orange peel. However, regarding PEI-3-220-2.5

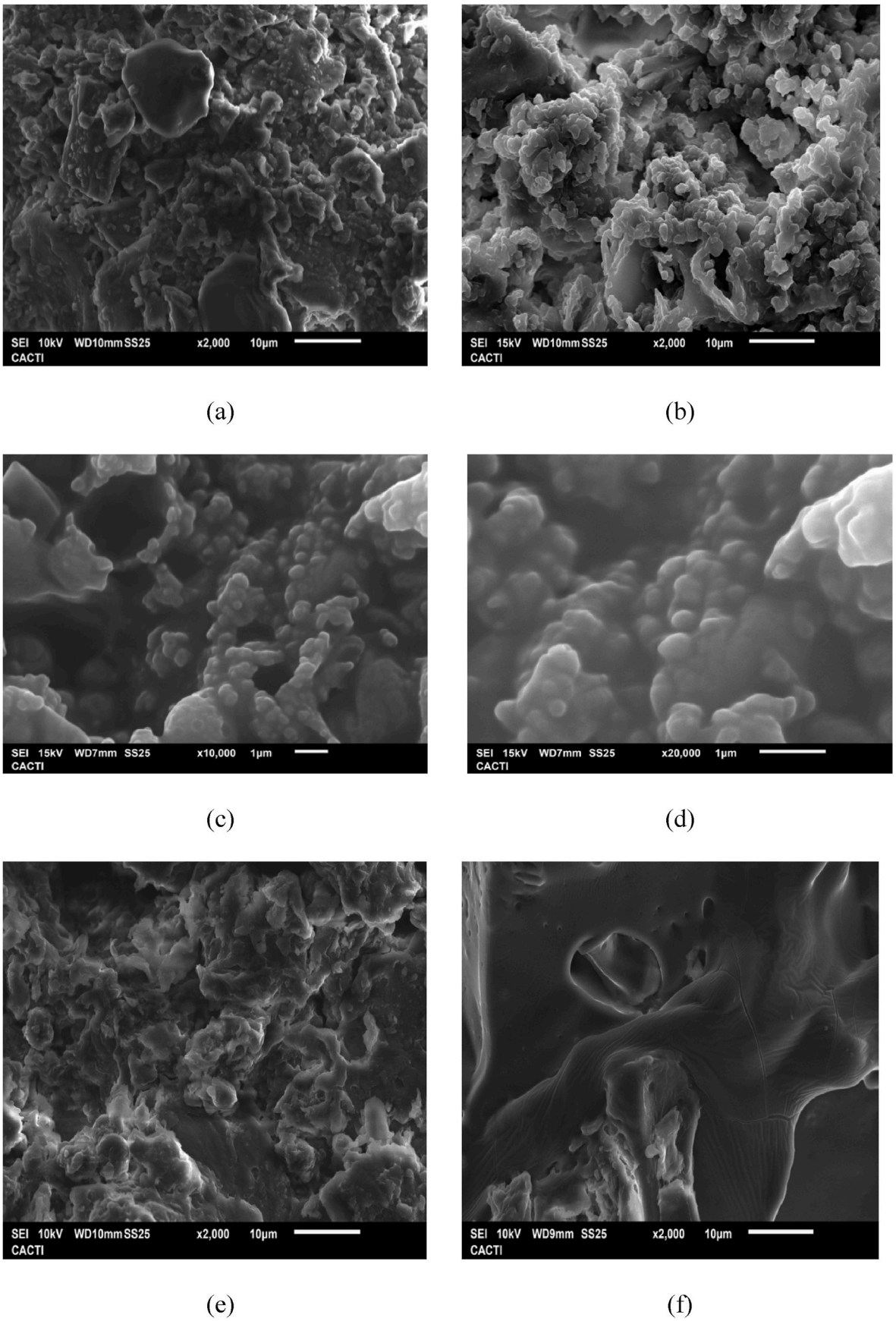

Fig. 3. SEM images capture from AL (a), 3-220-2.5 at different magnifications (b, c and d), U-3-220-2.5 (e) and PEI-3-220-2.5 (f).

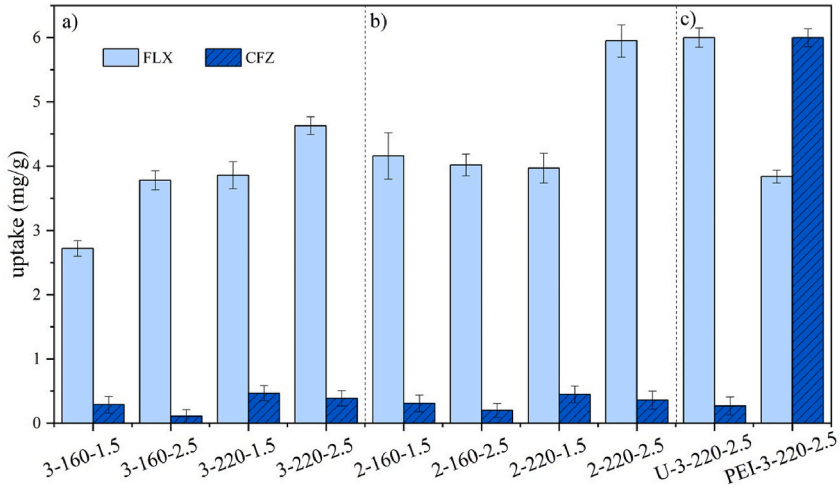

Fig. 4. Screening of the adsorption capacity of FLX and CFZ by all HC produced (a) W/AL ratio 3 and (b) W/AL ratio 2, (c) U-3-220-2.5 and PEI-3-220-2.5. Maximum potential adsorption of FLX or CFZ: 6 mg/g.

N-HC, the nitrogen content reported by Elsayed et al. (2022) was twice lower, probably because PEI was added in a post-treatment with glutaraldehyde as a crosslinker to a pine wood HC. This high nitrogen content of PEI-3-220-2.5 is most likely the cause of the very high PZC value of this N-HC, 9.7, while only 6.8 was recorded for U-3-220-2.5 (Table 1). Kasera et al. (2021) obtained similar PZC values for a pine bark biochar functionalized with U at 400 °C.

SEM images for U-3-220-2.5 and PEI-3-220-2.5 are shown in Fig. 3e and f respectively. For U-3-220-2.5, a surface with slightly smoother lines and appearance than the undoped HC is observed, suggesting that the U may be coating the surface and giving that appearance. Whereas for PEI-3-220-2.5, the surface is almost entirely covered by a smooth layer, clearly indicating the presence of the grafted polymer on the HC surface. No porosity can be observed in any of the N–HCs, which was confirmed by BET tests, which indicated that there was no porosity associated with any of these samples. Elsayed et al. (2022) reported a BET of only 3.8 m^2/g for an ozone oxidized HC doped with PEI (PEI-OzHC), which is in agreement with the findings in the current study.

In addition, SEM-EDX captures for U-3-220-2.5 and PEI-3-220-2.5 are presented in Fig ESM4a and ESM4b respectively in order to verify the spatial distribution of nitrogen in both N–HCs. As can be seen, both N–HCs presented a homogeneous nitrogen distribution over their surface, although it is true that the coverage of PEI-3-220-2.5 was denser, which is in line with the results of the previous elemental analysis.

FTIR comparative spectra for U-3-220-2.5, U and 3-220-2.5 are shown in Fig. 1b. The peaks associated with the lipids of the olive oil (2848, 2956 and 3005 cm^{-1}) remained in U-3-220-2.5, but their corresponding ester peak, 1738.9 cm^{-1} (Larkin, 2018), disappeared. However, a more intense peak related to the C═O bond stress mode of the O═C–NH amide group at 1647 cm^{-1}, emerged in this treatment suggesting a possible thermal ammonolysis reaction between triglycerides and the degradation product of U during the HTC process, ammonia (Zhu et al., 2021), to form an amide group (Griffin et al., 2013). Accompanying this amide peak, a band near 1593.1 cm^{-1} emerged corresponding to NH_2 bending and another near 1419.8 cm^{-1} being associated with C–N stretch. Besides, the doublet appearing at 3355. 4 and 3182.9 cm^{-1} indicate the stretches of NH_2 in primary amides. Additionally, the broad band between 800 and 630 cm^{-1} corresponds to the wagging vibration from primary and secondary amines (Larkin, 2018).

FTIR comparative spectra for PEI-3-220-2.5, PEI and 3-220-2.5 are shown in Fig. 1c. PEI shows a doublet at 3348 and 3195 cm^{-1} from primary amines (-NH_2) in the –NH stretching region, but a stronger peak at 3280 cm^{-1} from secondary amines (-NH), as the latter are in higher proportion in the polymer and no peak present in the region from tertiary amines. After the HTC treatment, only the 3280 cm^{-1} peak is present in PEI-3-220-2.5, suggesting the disappearance of primary amines in favor of secondary amines. Additionally, a strong peak at 1645 cm^{-1} appeared (O═C–NH), which suggests the formation of amides. In this case, a direct amide thermal formation (Charville et al., 2010), assisted by the carboxylic acids generated during the HTC process (Reza et al., 2014), was the most plausible reason for these changes. In addition to this, a strong peak at 1566 cm^{-1} corresponding to the CNH bend and the C–N stretch and the broad band from 800 to 730 cm^{-1} associated with primary and secondary amines and amides (Larkin, 2018) clearly present in PEI-3-220-2.5, indicates the increase of nitrogen content with respect to 3-220-2.5. The elevated PEI/AL ratio in PEI-3-220-2.5 and the lower intensity of peaks related to AL components suggest that PEI dominates the material and is presented in a crosslinked form due to the reactions in the HTC treatment.

On balance, primary amides can be found in U-3-220-2.5 and secondary amides dominated the PEI-3-220-2.5 spectrum. Thus, the grafting mechanism would be evident in both N–HCs.

To gain further information on surface chemistry, XPS analysis was carried out and the deconvoluted XPS C1s and N1s peaks and spectra of 3-220-2.5 and the N–HCs are shown in Tables ESM4 and ESM5 and represented in Fig ESM5. The accurate binding energies (BE) were determined by reference to the adventitious C1s peak at 285 eV and the experimental curves were fitted using a mix of Lorentzian-Gaussian lines in variable proportions. Table ESM4 shows a displacement of C–OH and C–O–C bonds (286.39 eV) at lower energies in N–HCs. This peak is characteristic of C–N bonds (285.97 and 286.06 eV) (Li et al., 2012), which appear in greater proportion in the PEI-3-220-2.5 (25.15%) sample than the U-3-220-2.5 (20.6%) due to the large number of bonds of this type contained in the PEI. In Both N–HCs appeared a different type of C-containing specie, the amide group (O═C–N, 287.6–288.3 eV), while O═C–O disappeared (288.88 eV), which corroborates the FTIR results. HC 3-220-2.5 showed no N-containing groups on the surface. N1s spectra (Table ESM5) of U-3-220-2.5 was deconvoluted in one type of N chemical environment, O═C–N on the surface (400.2 eV). PEI-3-220-2.5 N1s spectra could be resolved into four peaks secondary amino at 398.65 eV (32.51%), tertiary amino at 399.3 eV (41.46%), amide at 400.2 eV (31.19%), and nitrogen bounded oxygen species at 402.04 eV (3.53%). These results are similar to those reported by He et al. (2017) when preparing a hyperbranch-structured polyamine adsorbent for CO_2. Thus, XPS analysis confirmed the FTIR data obtained for both N–HCs and proved the success of the grafting process.

3.4. Adsorption of N–HCs

Adsorption tests for U-3-220-2.5 and PEI-3-220.2.5 are presented in Fig. 4c. At the initial concentration of 30 mg/L, U-3-220-2.5 did not show an improvement in CFZ adsorption and maintained the adsorption for FLX. On the other hand, PEI-3-220.2.5 presented a decrease in FLX adsorption; however, it presented an increase in CFZ adsorption of 1500% with respect to its parent, 3-220-2.5.

A more in-depth study to elucidate the adsorption process was carried out by fitting the experimental data to two isotherm models, Freundlich and Langmuir, and two kinetic models, PFO and PSO. The parameters obtained are detailed in Table 1 and the fittings represented in Fig. 5. PSO is the kinetic model that fitted the best for all N–HCs and pollutants. This would suggest chemical adsorption in which electrons are being shared or transferred between N–HCs and the pollutants, FLX and CFZ (Delgado-Moreno et al., 2021).

For U-3-220-2.5, Langmuir isotherm provided the best fit to the data for both contaminants, giving a maximum adsorption capacity of 111.63 mg/g for FLX and 16.09 mg/g for CFZ. This type of isotherm describes monolayer adsorption on a surface comprising a limited number of adsorption sites of uniform adsorption energies (Baccar et al., 2012). An increase in FLX adsorption by U-3-220-2.5 compared to the original 3-220-2.5 was observed. Chen et al. (2020) reported a maximum adsorption capacity for chlortetracycline of 44.3 mg/g using a furfural residue HC modified with urea.

Regarding PEI-3-220.2.5, Freundlich isotherm fitted well with the experimental data for both pollutants, as was the case for (Delgado-Moreno et al., 2021) using AL HC for adsorption, although the pharmaceuticals were different. It was found an outstanding experimental maximum uptake of 983.84 mg/g for CFZ and 29.31 mg/g for FLX. Even though Freundlich isotherm gave the best fit, the adjust was under 90% for CFZ, as it can be seen in Table 1 and Fig. 5d., The q_{max} parameter from Langmuir isotherm could be used as an estimate of the maximum adsorption capacity. Thus, maximum estimated adsorption capacities would be 34.24 mg/g for FLX and 1572.73 mg/g for CFZ. Freundlich model assumes heterogeneous surface energies and is influenced by the surface coverage (Baccar et al., 2012). Elsayed et al. (2022), prepared a PEI-OzHC in a post treatment with methanol and glutaraldehyde acting as crosslinker. The authors reported an uptake of 218.3 and 182.5 mg/g for Remazol Brilliant Blue R and Reactive Black 5, respectively. This

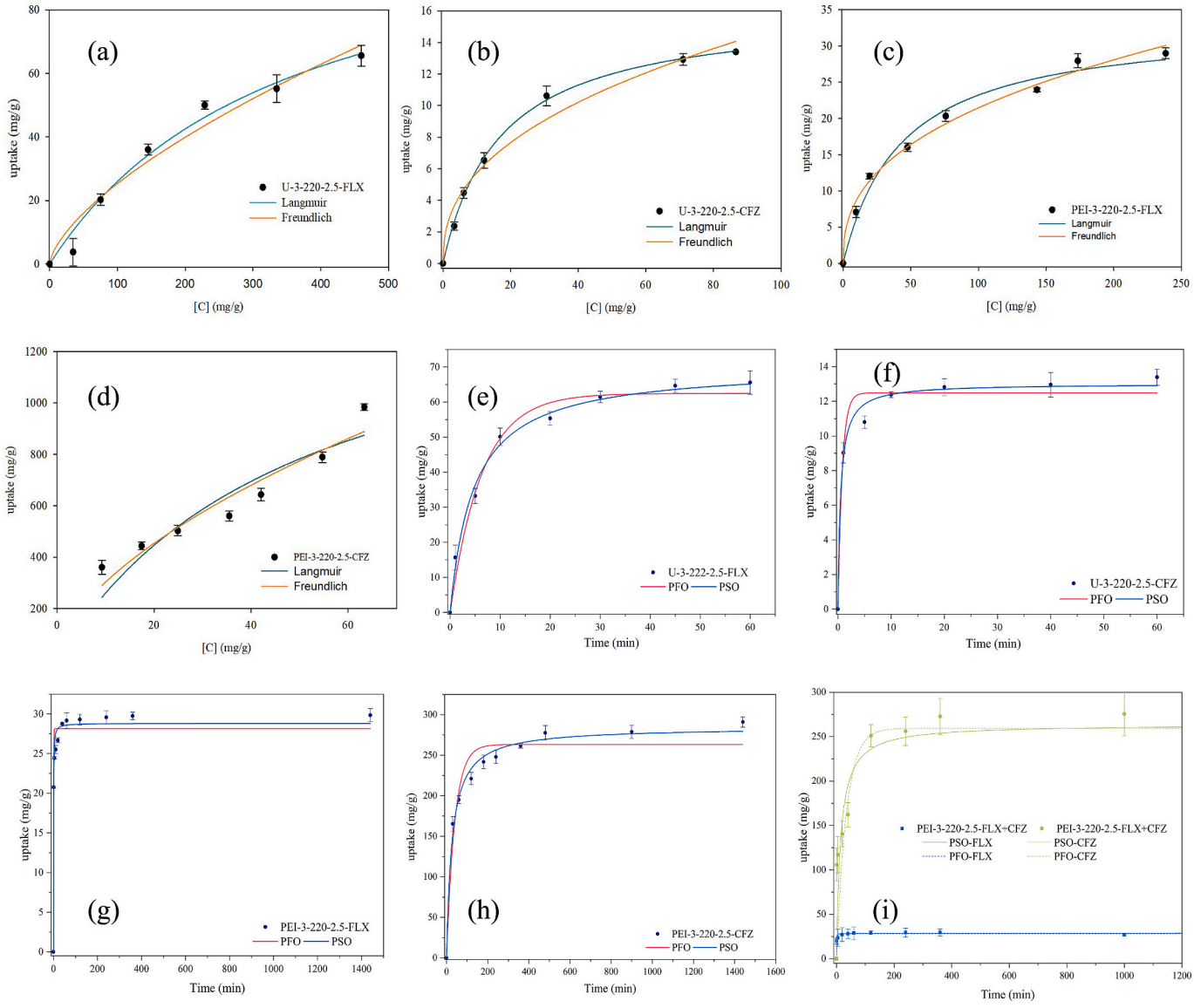

Fig. 5. Adsorption isotherms for U-3-220-2.5, FLX (a) and CFZ (b), and PEI-3-220-2.5, FLX (c) and CFZ (d). Kinetic models fittings for U-3-220-2.5, FLX (e) and CFZ (f), and PEI-3-220-2.5, FLX (g) and CFZ (h). Kinetic model fitting for PEI-3-220-2.5 co-adsorption FLX and CFZ (i).

great difference could be ascribed both to the suitability of the grafting procces presented in this study and to the PZC for PEI-OzHC adsorbent that was determined at pH 5.7. This fact results in a narrower adsorption pH-window (below 5.7) for both anionic dyes, in contrast to what is observed in the current study.

It is intriguing to conduct a comparative analysis of various studies that have utilized engineered adsorbents to remove pollutants from water, as they have demonstrated significant improvements in adsorption capacity despite utilizing varying techniques and modifiers (Adegoke et al., 2022; Ozelcaglayan and Parker, 2023; Shukla et al., 2023; Wang et al., 2023). One such study, conducted by Dolatabadi et al. (2021) involved the preparation of iron-modified activated carbon utilizing pistachio shells. Although the authors employed a more intricate methodology than that presented in this study, the adsorption efficiency improved significantly, with a change from 41.5% to 83.2% for acetamiprid. Similarly, another study by the same research group, Dolatabadi et al. (2022), focused on the development of a magnetic graphene oxide and carboxy methyl cellulose composite for pesticide removal, which resulted in a remarkable enhancement in the maximum adsorption capacity, from 20 to 30 mg/g of the raw materials to 108.3 mg/g for the composites. In summary, the studies discussed above offer evidence for the effectiveness of engineered bio-adsorbents in the development of versatile and cost-effective bio-adsorbents. The reported improvements in adsorption capacity demonstrate the potential of these approaches for the removal of pollutants from water.

3.4.1. Adsorption mechanism for U-3-220-2.5 and PEI-3-220-2.5

As previously mentioned for U-3-220-2.5, during the U-grafting process, amide groups are formed which could be related to this increase. In this sense, the adsorption capacity could be contributed both by electrostatic interactions and by amide-π bonding, frequently studied in pharmaceutical design (Imai et al., 2009). Nevertheless, electrostatic repulsion still exists between a negatively charged HC surface and CFZ^{-} as indicated by the low adsorption capacity predicted, since the influence of NH groups is not yet noticeable on PZC.

The incredibly high adsorption capacity showed by PEI-3-220-2.5 might be explained by the PZC exhibited (9.7, Table ESM2) which offers a positively charged surface. About 50% of the amino groups of PEI are protonated at the working pH and are distributed along the chain, giving it a high charge density (Ziebarth and Wang, 2010). This fact enables strong electrostatic attractions between these positively charged active sites and the negatively charged carboxyl groups of the CFZ, thereby promoting their adsorption. This mechanism has been reported by several authors while adsorbing metal anions in PEI-modified adsorbents (Deng and Ting, 2005). The possible mechanism of FLX adsorption on PEI-3-220-2.5 would be hydrogen bonding between the CF3 group (FLX) and the positively charged –NH groups of PEI-3-220-2.5, thereby mimicking one of the mechanisms of pharmaceutical adsorption in the body (Dalvit et al., 2014). However, adsorption is less favorable than in the case of CFZ, since the FLX molecule is positively charged and electrostatic repulsions may affect the adsorption process.

Given the good results obtained for PEI-3-220-2.5 for CFZ, a co-adsorption test of both pharmaceutical products was carried out in order to check if there were any interferences in the adsorption. As it can be seen in Fig. 5i, the adsorption capacity was maintained for both CFZ and FLX and the PSO kinetic model was the best fit to the experimental data. This result suggests that there were no interferences in the adsorption process between the two pharmaceuticals, probably indicating different binding sites.

4. Conclusions

N–HCs were successfully synthetized by grafting U and PEI onto the AL surface through a facile one-pot treatment. Elemental composition analysis confirmed that nitrogen atoms in the biomass were significantly increased in both cases but much more in the case of PEI-3-220-2.5. FTIR and XPS analyses performed on the surface of both N–HCs corroborated the presence of nitrogen groups in both cases, with amide groups appearing in the majority. U-3-220-2.5 improved the adsorption of FLX over its parent, but the functionalization was not sufficient for it to be versatile and adsorb both pharmaceuticals. On the other hand, PEI-3-220-2.5 showed a very high adsorption capacity for CFZ, although it had a clear drop in the adsorption of FLX with respect to the parent and that achieved with respect to U-3-220-2.5. Additionally, PEI-3-220-2.5 maintained its adsorption capacity for both pollutants in a co-adsorption test. Thus, PEI-3-220-2.5 proved to be a versatile adsorbent prepared in a simple way from an abundant lignocellulosic waste. Notwithstanding, further studies on stability and reusability for industrial applications should be carried out.

Credit author statement

Silvia Escudero-Curiel: Conceptualization, Methodology, Investigation, Validation, Formal analysis, Writing - original draft. **Marta Pazos**: Conceptualization, Supervision, Visualization, Writing – review & editing, Project administration, Funding acquisition. **Ángeles Sanromán**: Conceptualization, Supervision, Visualization, Writing – review & editing, Project administration, Funding acquisition.

Declaration of competing interest

The authors declare the following financial interests/personal relationships which may be considered as potential competing interests: As Maria Angeles Sanroman, a [co-]author on this paper, is one of the Guest Editor of this Special Issue, she was blinded to this paper during review, and the paper was independently handled by another Guest Editor.

Data availability

Data will be made available on request.

Acknowledgements

This research has been financially supported by Project PID 2020-113667GBI00 funded by MCIN/AEI/10.13039/501100011033 and PDC 2021-121394-I00 funded by MCIN/AEI/10.13039/501100011033 and by the European Union Next Generation EU/PRTR, Xunta de Galicia and European Regional Development Fund (ED431C 2021-43). Silvia Escudero-Curiel thanks Universidade de Vigo for her fellowship and the Universidade de Vigo/Consorcio Interuniversitario de Galicia (CISUG) for the open access charge. The authors are also grateful to Cristian Bolaño Losada for his technical support.

Appendix A. Supplementary data

Supplementary data to this article can be found online at https://doi.org/10.1016/j.envpol.2023.121751.

References

Abdelhadi, S.O., Dosoretz, C.G., Rytwo, G., Gerchman, Y., Azaizeh, H., 2017. Production of biochar from olive mill solid waste for heavy metal removal. Bioresour. Technol. 244, 759–767. https://doi.org/10.1016/J.BIORTECH.2017.08.013.

Adegoke, K.A., Adegoke, O.R., Araoye, A.O., Ogunmodede, J., Agboola, O.S., Bello, O.S., 2022. Engineered raw, carbonaceous, and modified biomass-based adsorbents for Rhodamine B dye removal from water and wastewater. Bioresour Technol Rep 18, 101082. https://doi.org/10.1016/J.BITEB.2022.101082.

Aharonov-Nadborny, R., Raviv, M., Graber, E.R., 2016. Soil spreading of liquid olive mill processing wastes impacts leaching of adsorbed terbuthylazine. Chemosphere 156, 220–227. https://doi.org/10.1016/J.CHEMOSPHERE.2016.04.104.

Ahmed, M.J., Hameed, B.H., 2018. Removal of emerging pharmaceutical contaminants by adsorption in a fixed-bed column: a review. Ecotoxicol. Environ. Saf. 149, 257–266. https://doi.org/10.1016/j.ecoenv.2017.12.012.

Ahmed, W., Mehmood, S., Mahmood, M., Ali, S., Shakoor, A., Núñez-Delgado, A., Asghar, R.M.A., Zhao, H., Liu, W., Li, W., 2023. Adsorption of Pb(II) from wastewater using a red mud modified rice-straw biochar: influencing factors and reusability. Environ. Pollut. 326, 121405 https://doi.org/10.1016/J.ENVPOL.2023.121405.

Alburquerque, J.A., Gonzálvez, J., García, D., Cegarra, J., 2004. Agrochemical characterisation of "alperujo". a solid by-product of the two-phase centrifugation method for olive oil extraction. Bioresour Technol 91, 195–200. https://doi.org/10.1016/S0960-8524(03)00177-9.

Arrigo, R., Hävecker, M., Wrabetz, S., Blume, R., Lerch, M., McGregor, J., Parrott, E.P.J., Zeitler, J.A., Gladden, L.F., Knop-Gericke, A., Schlögl, R., Su, D.S., 2010. Tuning the acid/base properties of nanocarbons by functionalization via amination. J. Am. Chem. Soc. 132, 9616–9630. https://doi.org/10.1021/JA910169V.

Atallah, E., Kwapinski, W., Ahmad, M.N., Leahy, J.J., Zeaiter, J., 2019. Effect of water-sludge ratio and reaction time on the hydrothermal carbonization of olive oil mill wastewater treatment: hydrochar characterization. J. Water Process Eng. 31, 100813 https://doi.org/10.1016/j.jwpe.2019.100813.

Baccar, R., Sarrà, M., Bouzid, J., Feki, M., Blánquez, P., 2012. Removal of pharmaceutical compounds by activated carbon prepared from agricultural by-product. Chem. Eng. J. 211–212, 310–317. https://doi.org/10.1016/J.CEJ.2012.09.099.

Barjasteh-Askari, F., Davoudi, M., Dolatabadi, M., Ahmadzadeh, S., 2021. Iron-modified activated carbon derived from agro-waste for enhanced dye removal from aqueous solutions. Heliyon 7, e07191. https://doi.org/10.1016/j.heliyon.2021.e07191.

Benavente, V., Calabuig, E., Fullana, A., 2015. Upgrading of moist agro-industrial wastes by hydrothermal carbonization. J. Anal. Appl. Pyrolysis 113, 89–98. https://doi.org/10.1016/j.jaap.2014.11.004.

Capobianco, L., di Caprio, F., Altimari, P., Astolfi, M.L., Pagnanelli, F., 2020. Production of an iron-coated adsorbent for arsenic removal by hydrothermal carbonization of olive pomace: effect of the feedwater pH. J. Environ. Manag. 273, 111164 https://doi.org/10.1016/j.jenvman.2020.111164.

Charville, H., Jackson, D., Hodges, G., Whiting, A., 2010. The thermal and boron-catalysed direct amide formation reactions: mechanistically understudied yet important processes. Chem. Commun. 46, 1813–1823. https://doi.org/10.1039/B923093A.

Chen, X., Li, H., Liu, W., Meng, Z., Wu, Z., Wang, G., Liang, Y., Bi, S., 2020. Low-temperature constructing N-doped graphite-like mesoporous structure biochar from furfural residue with urea for removal of chlortetracycline from wastewater and hydrothermal catalytic degradation mechanism. Colloids Surf. A Physicochem. Eng. Asp. 600, 124873 https://doi.org/10.1016/j.colsurfa.2020.124873.

Choudhary, V., Philip, L., 2022. Sustainability assessment of acid-modified biochar as adsorbent for the removal of pharmaceuticals and personal care products from secondary treated wastewater. J. Environ. Chem. Eng. 10, 107592 https://doi.org/10.1016/J.JECE.2022.107592.

Dalvit, C., Invernizzi, C., Vulpetti, A., 2014. Fluorine as a hydrogen-bond acceptor: experimental evidence and computational calculations. Chem. Eur J. 20, 11058–11068. https://doi.org/10.1002/CHEM.201402858.

Delgado-Moreno, L., Bazhari, S., Gasco, G., Méndez, A., el Azzouzi, M., Romero, E., 2021. New insights into the efficient removal of emerging contaminants by biochars and hydrochars derived from olive oil wastes. Sci. Total Environ. 752, 141838 https://doi.org/10.1016/j.scitotenv.2020.141838.

Deng, S., Ting, Y.P., 2005. Polyethylenimine-modified fungal biomass as a high-capacity biosorbent for Cr(VI) anions: sorption capacity and uptake mechanisms. Environ. Sci. Technol. 39, 8490–8496. https://doi.org/10.1021/es050697u.

Dolatabadi, M., Naidu, H., Ahmadzadeh, S., 2022. Adsorption characteristics in the removal of chlorpyrifos from groundwater using magnetic graphene oxide and carboxy methyl cellulose composite. Sep. Purif. Technol. 300, 121919 https://doi.org/10.1016/J.SEPPUR.2022.121919.

Dolatabadi, M., Naidu, H., Ahmadzadeh, S., 2021. A green approach to remove acetamiprid insecticide using pistachio shell-based modified activated carbon; economical groundwater treatment. J. Clean. Prod. 316, 128226 https://doi.org/10.1016/J.JCLEPRO.2021.128226.

Ebele, A.J., Abou-Elwafa Abdallah, M., Harrad, S., 2017. Pharmaceuticals and personal care products (PPCPs) in the freshwater aquatic environment. Emerg Contam 3, 1–16. https://doi.org/10.1016/j.emcon.2016.12.004.

Elsayed, I., Madduri, S., El-Giar, E.M., Hassan, E.B., 2022. Effective removal of anionic dyes from aqueous solutions by novel polyethylenimine-ozone oxidized hydrochar (PEI-OzHC) adsorbent. Arab. J. Chem. 15, 103757 https://doi.org/10.1016/j.arabjc.2022.103757.

Ewadh, H.M., Abdullah, S.R., Anwar, N., Hasan, H.A., 2017. Pharmaceuticals and personal care products : sources , toxicity in the environment , regulations and removal Technologies. J. Chem. Pharmaceut. Sci. https://doi.org/10.30558/jchps.

Gimenez, M., Rodríguez, M., Montoro, L., Sardella, F., Rodríguez-Gutierrez, G., Monetta, P., Deiana, C., 2020. Two phase olive mill waste valorization. Hydrochar production and phenols extraction by hydrothermal carbonization. Biomass Bioenergy 143, 105875. https://doi.org/10.1016/j.biombioe.2020.105875.

González, B., Manyà, J.J., 2020. Activated olive mill waste-based hydrochars as selective adsorbents for CO2 capture under postcombustion conditions. Chemical Engineering and Processing - Process Intensification 149, 107830. https://doi.org/10.1016/j.cep.2020.107830.

Griffin, J., Atherton, J., Page, M.I., 2013. The ammonolysis of esters in liquid ammonia. J. Phys. Org. Chem. 26, 1032–1037. https://doi.org/10.1002/poc.3148.

He, H., Hu, Y., Chen, S., Zhuang, L., Ma, B., Wu, Q., 2017. Preparation and properties of A hyperbranch-structured polyamine adsorbent for carbon dioxide capture. Sci. Rep. 7, 1–10. https://doi.org/10.1038/s41598-017-04329-w.

Huang, Q., Liu, M., Zhao, J., Chen, J., Zeng, G., Huang, H., Tian, J., Wen, Y., Zhang, X., Wei, Y., 2018. Facile preparation of polyethylenimine-tannins coated SiO2 hybrid materials for Cu2+ removal. Appl. Surf. Sci. 427, 535–544. https://doi.org/10.1016/J.APSUSC.2017.08.233.

Imai, Y.N., Inoue, Y., Nakanishi, I., Aura, K.K., 2009. Amide-π interactions between formamide and benzene. J. Comput. Chem. 30, 2267–2276. https://doi.org/10.1002/JCC.21212.

Jiang, Q., Xie, W., Han, S., Wang, Y., Zhang, Y., 2019. Enhanced adsorption of Pb(II) onto modified hydrochar by polyethyleneimine or H3PO4: an analysis of surface property and interface mechanism. Colloids Surf. A Physicochem. Eng. Asp. 583, 123962 https://doi.org/10.1016/j.colsurfa.2019.123962.

Kasera, N., Hall, S., Kolar, P., 2021. Effect of surface modification by nitrogen-containing chemicals on morphology and surface characteristics of N-doped pine bark biochars. J. Environ. Chem. Eng. 9, 105161 https://doi.org/10.1016/j.jece.2021.105161.

Larkin, P.J., 2018. Introduction. In: Infrared and Raman Spectroscopy. Elsevier, pp. 1–5. https://doi.org/10.1016/b978-0-12-804162-8.00001-x.

Li, Y., Zhao, Y., Cheng, H., Hu, Y., Shi, G., Dai, L., Qu, L., 2012. Nitrogen-doped graphene quantum dots with oxygen-rich functional groups. J. Am. Chem. Soc. 134 https://doi.org/10.1021/ja206030c.

Libra, J.A., Ro, K.S., Kammann, C., Funke, A., Berge, N.D., Neubauer, Y., Titirici, M.M., Fühner, C., Bens, O., Kern, J., Emmerich, K.H., 2014. Hydrothermal Carbonization of Biomass Residuals: a Comparative Review of the Chemistry, Processes and Applications of Wet and Dry Pyrolysis, pp. 71–106. https://doi.org/10.4155/BFS.10.81.

Liu, Z., Zhang, F.S., Wu, J., 2010. Characterization and application of chars produced from pinewood pyrolysis and hydrothermal treatment. Fuel 89, 510–514. https://doi.org/10.1016/J.FUEL.2009.08.042.

Melchor-Martínez, E.M., Jiménez-Rodríguez, M.G., Martínez-Ruiz, M., Peña-Benavides, S.A., Iqbal, H.M.N., Parra-Saldívar, R., Sosa- Hernández, J.E., 2021. Antidepressants surveillance in wastewater: overview extraction and detection. Case Studies in Chemical and Environmental Engineering 3, 100074. https://doi.org/10.1016/j.cscee.2020.100074.

Missaoui, A., Bostyn, S., Belandria, V., Cagnon, B., Sarh, B., Gökalp, I., 2017. Hydrothermal carbonization of dried olive pomace: energy potential and process performances. J. Anal. Appl. Pyrolysis 128, 281–290. https://doi.org/10.1016/j.jaap.2017.09.022.

Mohan, D., Sarswat, A., Ok, Y.S., Pittman, C.U., 2014. Organic and inorganic contaminants removal from water with biochar, a renewable, low cost and sustainable adsorbent – a critical review. Bioresour. Technol. 160, 191–202. https://doi.org/10.1016/j.biortech.2014.01.120.

Mumme, J., Eckervogt, L., Pielert, J., Diakité, M., Rupp, F., Kern, J., 2011. Hydrothermal carbonization of anaerobically digested maize silage. Bioresour. Technol. 102, 9255–9260. https://doi.org/10.1016/j.biortech.2011.06.099.

Opatokun, S.A., Kan, T., al Shoaibi, A., Srinivasakannan, C., Strezov, V., 2015. Characterization of food waste and its digestate as feedstock for thermochemical processing. Energy Fuel. 30, 1589–1597. https://doi.org/10.1021/ACS.ENERGYFUELS.5B02183.

Ozelcaglayan, E.D., Parker, W.J., 2023. β-Cyclodextrin functionalized adsorbents for removal of organic micropollutants from water. Chemosphere 320, 137964. https://doi.org/10.1016/J.CHEMOSPHERE.2023.137964.

Popescu, M-C., Froidevaux, .J, Navi, P., Popescu, C-M., 2013. Structural modifications of Tilia cordata wood during heat treatment investigated by FT-IR and 2D IR correlation spectroscopy. Journal of Molecular Structure 1033, 176–186. https://doi.org/10.1016/j.molstruc.2012.08.035.

Qu, J., Bi, F., Hu, Q., Wu, P., Ding, B., Tao, Y., Ma, S., Qian, C., Zhang, Y., 2023. A novel PEI-grafted N-doping magnetic hydrochar for enhanced scavenging of BPA and Cr (VI) from aqueous phase. Environ. Pollut. 321, 121142 https://doi.org/10.1016/J.ENVPOL.2023.121142.

Rajapaksha, A.U., Chen, S.S., Tsang, D.C.W., Zhang, M., Vithanage, M., Mandal, S., Gao, B., Bolan, N.S., Ok, Y.S., 2016. Engineered/designer biochar for contaminant removal/immobilization from soil and water: potential and implication of biochar modification. Chemosphere 148, 276-291. https://doi.org/10.1016/j.chemosphere.2016.01.043.

Rajapaksha, A.U., Dilrukshi Premarathna, K.S., Gunarathne, V., Ahmed, A., Vithanage, M., 2019. Sorptive removal of pharmaceutical and personal care products from water and wastewater. In: Pharmaceuticals and Personal Care Products: Waste Management and Treatment Technology Emerging Contaminants and Micro Pollutants. Elsevier, pp. 213–238. https://doi.org/10.1016/B978-0-12-816189-0.00009-3.

Reza, M.T., Andert, J., Wirth, B., Busch, D., Pielert, J., Lynam, J.G., Mumme, J., 2014. Hydrothermal carbonization of biomass for energy and crop production. Appl. Bioenergy 1, 11–29. https://doi.org/10.2478/apbi-2014-0001.

Rinaldi, M., Rana, G., Introna, M., 2003. Olive-mill wastewater spreading in southern Italy: effects on a durum wheat crop. Field Crop. Res. 84, 319–326. https://doi.org/10.1016/S0378-4290(03)00097-2.

Román, S., Nabais, J.M.V., Ledesma, B., Laginhas, C., Titirici, M.M., 2020. 2020. Surface interactions during the removal of emerging contaminants by hydrochar-based adsorbents. Molecules 25, 2264. https://doi.org/10.3390/MOLECULES25092264. Page 2264 25.

Rosli, N., Ngadi, N., Azman, M.A., 2019. Synthesis of modified spent tea for aspirin adsorption in aqueous solution. Int. J. Recent Technol. Eng. 8, 531–534. https://doi.org/10.35940/ijrte.A3502.098319.

Saha, N., Saba, A., Reza, M.T., 2019. Effect of hydrothermal carbonization temperature on pH, dissociation constants, and acidic functional groups on hydrochar from cellulose and wood. J. Anal. Appl. Pyrolysis 137, 138–145. https://doi.org/10.1016/J.JAAP.2018.11.018.

Shukla, V., Panchal, D., Prakash, O., Mondal, P., Hiwrale, I., Dhodapkar, R.S., Pal, S., 2023. Magnetically engineered sulfurized peat-based activated carbon for

remediation of emerging pharmaceutical contaminants. Bioresour. Technol. 369, 128399 https://doi.org/10.1016/J.BIORTECH.2022.128399.
Volpe, M., Fiori, L., 2017. From olive waste to solid biofuel through hydrothermal carbonisation: the role of temperature and solid load on secondary char formation and hydrochar energy properties. J. Anal. Appl. Pyrolysis 124, 63–72. https://doi.org/10.1016/j.jaap.2017.02.022.
Volpe, M., Wüst, D., Merzari, F., Lucian, M., Andreottola, G., Kruse, A., Fiori, L., 2018. One stage olive mill waste streams valorisation via hydrothermal carbonisation. Waste Manag. 80, 224–234. https://doi.org/10.1016/j.wasman.2018.09.021.
Wang, T., Zhai, Y., Zhu, Y., Li, C., Zeng, G., 2018. A review of the hydrothermal carbonization of biomass waste for hydrochar formation: process conditions, fundamentals, and physicochemical properties. Renew. Sustain. Energy Rev. 90, 223–247. https://doi.org/10.1016/J.RSER.2018.03.071.
Wang, Y., Wang, F., Shu, L., Wu, P., Li, Z., Gao, J., Liu, H., 2023. Novel sustainable adsorbents prepared by banana/pomegranate peels via EDTA grafting for effective removal of Cd(II), Co(II), Mn(II), and Ni(II) from sewage system. Water Air Soil Pollut. 234, 1–16. https://doi.org/10.1007/S11270-023-06101-5/FIGURES/6.
Xia, Y., Luo, H., Li, D., Chen, Z., Yang, S., Liu, Z., Yang, T., Gai, C., 2020. Efficient immobilization of toxic heavy metals in multi-contaminated agricultural soils by amino-functionalized hydrochar: performance, plant responses and immobilization mechanisms. Environ. Pollut. 261, 114217 https://doi.org/10.1016/j.envpol.2020.114217.
Xiao, K., Liu, H., Li, Y., Yang, G., Wang, Y., Yao, H., 2020. Excellent performance of porous carbon from urea-assisted hydrochar of orange peel for toluene and iodine adsorption. Chem. Eng. J. 382, 122997 https://doi.org/10.1016/j.cej.2019.122997.
Xie, J., Liu, M., He, M., Liu, Y., Li, J., Yu, F., Lv, Y., Lin, C., Ye, X., 2023. Ultra-efficient adsorption of diclofenac sodium on fish-scale biochar functionalized with H3PO4 via synergistic mechanisms. Environ. Pollut. 322, 121226 https://doi.org/10.1016/J.ENVPOL.2023.121226.
Xu, F., Yu, J., Tesso, T., Dowell, F., Wang, D., 2013. Qualitative and quantitative analysis of lignocellulosic biomass using infrared techniques: a mini-review. Appl. Energy 104, 801–809. https://doi.org/10.1016/J.APENERGY.2012.12.019.
Yang, G., Chen, H., Qin, H., Feng, Y., 2014. Amination of activated carbon for enhancing phenol adsorption: effect of nitrogen-containing functional groups. Appl. Surf. Sci. 293, 299–305. https://doi.org/10.1016/j.apsusc.2013.12.155.
Zhu, N., Qian, F., Xu, X., Wang, M., Teng, Q., 2021. Thermogravimetric experiment of urea at constant temperatures. Materials 14. https://doi.org/10.3390/MA14206190.
Ziebarth, J.D., Wang, Y., 2010. Understanding the protonation behavior of linear polyethylenimine in solutions through Monte Carlo simulations. Biomacromolecules 11, 29. https://doi.org/10.1021/BM900842D.